Supplemental Document


# Full-field x-ray fluorescence imaging using a Fresnel zone plate coded aperture: supplement

**JAKOB SOLTAU,[1,4,†] PAUL MEYER,[1,5,†] ROBERT HARTMANN,[2] LOTHAR STRÜDER,[2] HEIKE SOLTAU,[3] AND TIM SALDITT[1,*]**

[1] *Institut für Röntgenphysik, Georg-August-Universität Göttingen, Friedrich-Hund-Platz 1, Göttingen, Germany*
[2] *PNSensor, Otto-Hahn-Ring 6, München, Germany*
[3] *PNDetector, Otto-Hahn-Ring 6, München, Germany*
[4] *e-mail: jakob.soltau@uni-goettingen.de*
[5] *e-mail: paul.meyer@uni-goettingen.de*
[*] *Corresponding author: tsaldit@gwdg.de*
[†] *These authors contributed equally to this work.*



Supplement DOI: https://doi.org/10.6084/m9.figshare.21680408

Parent Article DOI: https://doi.org/10.1364/OPTICA.477809

# Supplemental Material: Laboratory-based full-field x-ray fluorescence imaging using a Fresnel zone plate

**Jakob Soltau,[1,*] Paul Meyer,[1,*] Robert Hartmann,[2] Lothar Strüder,[2] Heike Soltau,[3] and Tim Saldit[1,+]**

[1] *Institut für Röntgenphysik, Georg-August-Universität Göttingen, Friedrich-Hund-Platz 1, Göttingen, Germany*
[2] *PNSensor, Otto-Hahn-Ring 6, München, Germany*
[3] *PNDetector, Otto-Hahn-Ring 6, München, Germany*
[*] *equal contribution,* [+] *jakob.soltau@uni-goettingen.de, paul.meyer@uni-goettingen.de, tsaldit@gwdg.de*

## 1. SEM images of the sample

Fig. 1 shows scanning electron microscope (SEM) images of the Ti- and Fe-samples used in the experiment. The structures were two grids with a line width of (a) 100 µm and (b) 50 µm, and (c) dots with a diameter of 50 µm. The structure height of all samples was 550 nm. The gray value of the color coding depends on the material. Slightly darker gray values correspond to the Ti-structures and the lighter gray values to the Fe-structures. The samples were fabricated in-house by e-beam lithography (eLine, Raith, Dortmund, Germany) on a single Si-wafer, using PMMA resist and a lift-off process of the evaporated Ti- and subsequently Fe-layers.

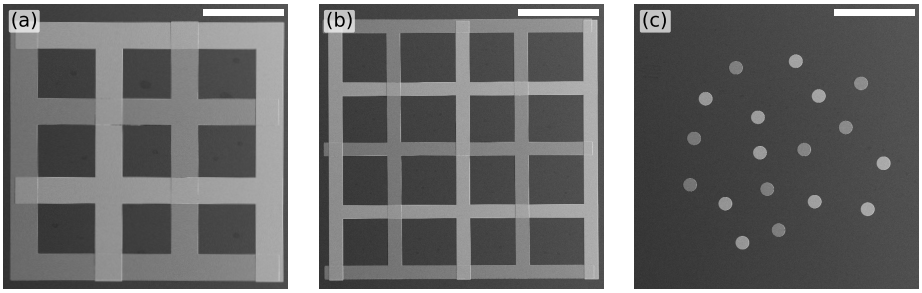


Fig. 1. The different sample structures imaged with an SEM: two grids with a line width of (a) 100 µm and (b) 50 µm, and (c) dots with a diameter of 50 µm. The structure height of all samples was 550 nm. Scale bars: 300 µm

## 2. Calculation of the resolution

The resolution was quantified based on the reconstructions presented in Fig. 4 (e,f) of the main manuscript and shown here in Fig. 2 for (a) the Ti-structure and (b) Fe-structure. The image shows the grid-structure with line-widths of 100 µm. The images were reconstructed from three recordings of $F = 1.43 \times 10^{-3}$ ($z_{01} = 13.9$ mm), $F = 1.96 \times 10^{-3}$ ($z_{01} = 16.3$ mm) and $F = 2.66 \times 10^{-3}$ ($z_{01} = 19.0$ mm) respectively, each recorded with an exposure time of 2 h. The reconstruction was performed using the multi-distance CTF approach. The resolution was determined by fitting an error-function at one grid-line in (a) and (b) respectively. The profile of the lines were determined by the average of 7 pixel rows. The positions of the line profiles are indicated by a blue bar in (a) and (b). The resulting profiles were fitted to the difference of two error functions $\Phi(x) \cdot \mathrm{s\mu m}^2 = a \cdot (\mathrm{erf}((x - x_1)/s) - \mathrm{erf}((x - x_2)/s)) + b$. Fig. 2 (c,d) show the corresponding line-profiles and the fitted error-functions. The results indicate a resolution of 34(6) µm (Ti) and 36(7) µm (Fe) (half width at half maximum of the Gaussian PSF). This gives

a mean resolution of about 35 µm (HWHM). Given the outermost FZP zone width of 25 µm, the result is as expected.

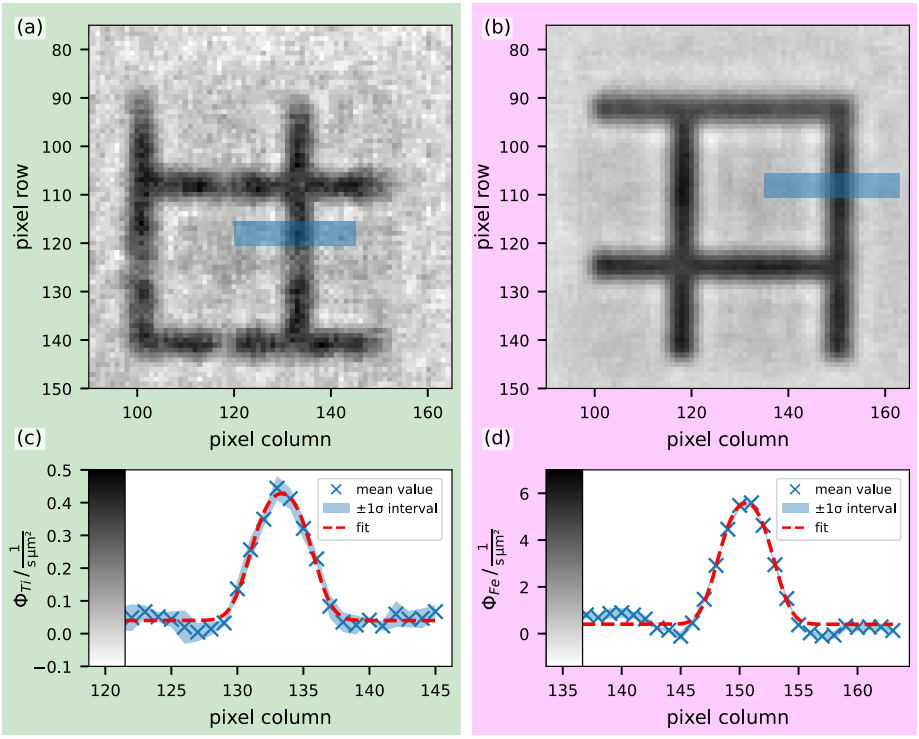


Fig. 2. Reconstruction of the (a) Ti- and (b) Fe-structure using three exposures with the FZP positioned at different distances $z_{01}$ corresponding to $F = 1.43 \times 10^{-3}$ ($z_{01}$ = 13.9 mm), $F = 1.96 \times 10^{-3}$ ($z_{01}$ = 16.3 mm) and $F = 2.66 \times 10^{-3}$ ($z_{01}$ = 19.0 mm). The total illumination time was 6 h. The bar indicates the position of the data extracted for the fitted error functions. The effective pixel size in the reconstruction is 18.5 µm. (c) & (d) The reconstructed data points and the fitted error function. The average was taken over 7 pixel rows and the resulting profile fitted to the difference of two error functions. The results indicate a resolution of 34(6) µm for Ti and 36(7) µm for Fe (half width at half maximum of the Gaussian PSF).

## 3. Sub-pixel resolution

The pnCCD-detector can be used to calculate the position of single photons depending on the charge distribution in neighboring pixels of the pnCCD-detector [1]. This enables a higher spatial resolution than given by the physical pixel size of 48 µm. The calculation of a sub-pixel resolution is of importance for the case that the smallest features of the structure can not be resolved, given the size of the detector pixels. This depends on the magnification $M_{\mathrm{obj}}$ and the size of the smallest FZP-zone $\Delta_r$. For the calculation of the sub-pixel position different approaches can be applied [1, 2]. We performed here a rather simple approach using the centroid of the charge since we decrease the pixel size only by a factor of two to 24 µm. Fig. 3 shows first results, comparing reconstructions of the 50 µm-dot structures, without (a,b) and with (c,d) sub-pixel resolution for the Ti- and Fe-materials respectively. The reconstruction is based on an image recorded at $F = 2.66 \times 10^{-3}$ ($z_{01}$ = 19.0 mm) with an exposure time of 2 h. The

sub-pixel calculation indicates an improved resolution. Especially the Fe-dots appear rounder and less pixellated. However, the denser sampling also reduces the signal-to-noise-ratio due to the decreased flux per pixel. This shows that the sub-pixel calculation can be beneficial when, (i) a FZP with smaller zones is used to achieve a higher resolution, or (ii) if the sample, FZP and detector are placed more closely together to increase the solid angle of emission captured Σ.

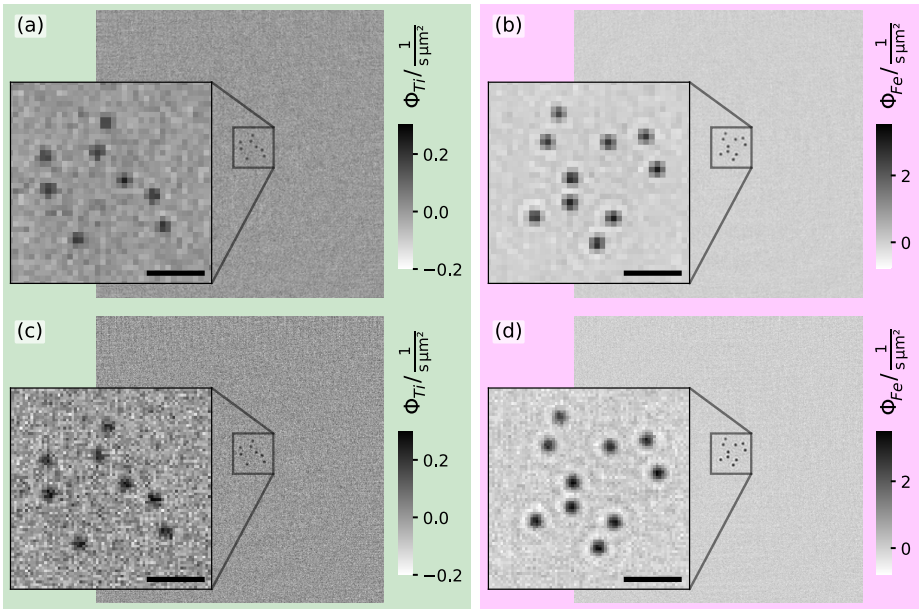


Fig. 3. Comparison of results using the sub-pixel resolution and the conventional reconstruction approach. (a) The conventional reconstruction of the Ti-structures and (b) Fe-structures. (c) The sub-pixel reconstruction of the Ti-structures and (d) Fe-structures. In case of (a,b) the effective pixel size is 30 µm, and for (c,d) 15 µm. The sample was the 50 µm-dot structures, positioned at $F = 2.66 \times 10^{-3}$ ($z_{01} = 19.0\,\mathrm{mm}$) and recorded with an exposure time of 2 h. Scale bars: 300 µm

## 4. Photon counts

From the acquired holograms, the photon emission flux $\Phi$ of the sample was reconstructed, as shown in the main article. For easier comparison of the photon statistics with the pinhole acquisition and for the determination of statistical errors, it is useful to convert to an image $\tilde{I}^{\mathrm{ZP}}$ representing the detected photons for each pixel, assuming that all photons crossing the zone plate reach the detector. Taking into account the acquisition time $T$, the detector pixel size px, the geometric magnification $M_{\mathrm{obj}}$ of the sample, the radius $r_{\mathrm{ZP}}$ of the zone plate and its distance $z_{01}$ from the sample, both representations are related by

$$\tilde{I}^{ZP} = \Phi \cdot \underbrace{T}_{\text{acquisition time}} \cdot \underbrace{(\mathrm{px}/M_{\mathrm{obj}})^2}_{\text{effective pixel area}} \cdot \underbrace{\frac{1/2 \cdot \pi r_{\mathrm{ZP}}^2}{4\pi z_{01}^2}}_{\substack{\simeq \text{ solid angle} \\ \text{of the zone plate}}} \tag{1}$$

Fig. 4 shows $\tilde{I}^{\mathrm{ZP}}$ in addition to the acquired holograms for the measurement depicted in Fig. 4 of the main manuscript.

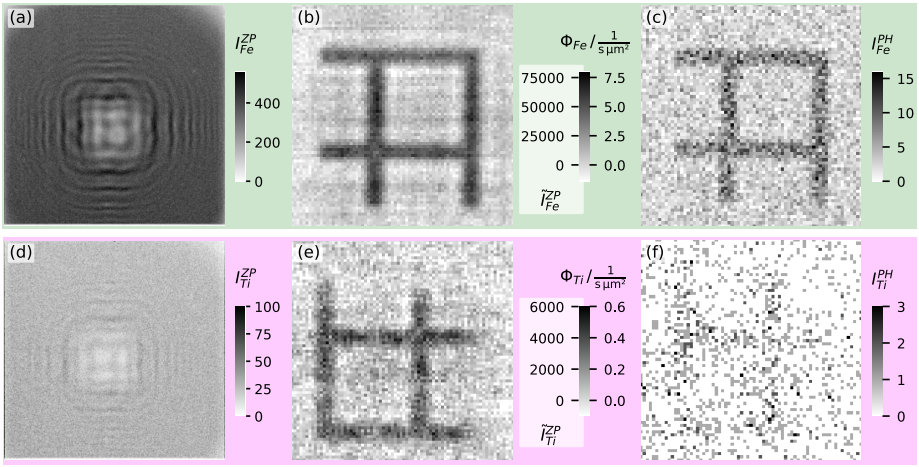


Fig. 4. Comparison of photon statistics of the single distance acquisitions shown in Fig. 4 of the main manuscript. (a) Photon counts of the acquired Fe hologram. (b) Fe reconstruction. The added scaling $\tilde{I}^{\mathrm{ZP}}_{\mathrm{Fe}}$ shows represented photon counts per pixel. (c) Fe pinhole photon counts. (c), (d) & (e): Respective images for the Ti-signal.

## References

1. I. Ordavo, S. Ihle, V. Arkadiev, O. Scharf, H. Soltau, A. Bjeoumikhov, S. Bjeoumikhova, G. Buzanich, R. Gubzhokov, A. Günther, R. Hartmann, P. Holl, N. Kimmel, M. Kühbacher, M. Lang, N. Langhoff, A. Liebel, M. Radtke, U. Reinholz, H. Riesemeier, G. Schaller, F. Schopper, L. Strüder, C. Thamm, and R. Wedell, "A new pnccd-based color x-ray camera for fast spatial and energy-resolved measurements," Nucl. Instruments Methods Phys. Res. Sect. A: Accel. Spectrometers, Detect. Assoc. Equip. **654**, 250–257 (2011).
2. B. Eckert, S. Aschauer, P. Holl, P. Majewski, T. Zabel, and L. Strüder, "Electron imaging reconstruction for pixelated semiconductor tracking detectors in transmission electron microscopes using the approach of convolutional neural networks," IEEE Transactions on Nucl. Sci. **69**, 1014–1021 (2022).